

Titanium Oxide and their Effects on Structure, Physical Properties and Electrochemical Corrosion Parameters of Alloys

Abu Bakr El- Bediwi^{1*}, Eman Kashita², Feryal Dawood³ and Fathia Khalifa⁴

¹Metal Physics Lab, Physics Department, Faculty of Science, Mansoura University, Mansoura, Egypt

²Educational Services, Qassim University, Ministry of High Education, Kingdom of Saudi Arabia

³Basic education college, University of Diayala, Iraq

⁴Sirte University, Sirte, Libya

ISSN: 2576-8840



*Corresponding author: Abu Bakr El-Bediwi, Physics Department, Faculty of Science, Mansoura University, Mansoura, Egypt

Submission: 📅 November 03, 2019

Published: 📅 November 12, 2019

Volume 12 - Issue 2

How to cite this article: Abu Bakr El-Bediwi, Eman Kashita, Feryal Dawood, Fathia Khalifa. Titanium Oxide and their Effects on Structure, Physical Properties and Electrochemical Corrosion Parameters of Alloys. Res Dev Material Sci. 12(2). RDMS.000784.2019. DOI: [10.31031/RDMS.2019.12.000784](https://doi.org/10.31031/RDMS.2019.12.000784)

Copyright@ Abu Bakr El- Bediwi, This article is distributed under the terms of the Creative Commons Attribution 4.0 International License, which permits unrestricted use and redistribution provided that the original author and source are credited.

Abstract

Effect of adding titanium oxide nanoparticles to bismuth or tin based alloys on microstructure, physical properties and corrosion parameters has been studied. Surface properties of tin or bismuth alloys such as hardness and corrosion parameters improved after adding titanium oxide. Matrix structure of tin or bismuth alloys changed after adding titanium oxide due to form a solid solution with caused a lattice distortion or growth formed phases. A little variation caused in melting temperature for bismuth or tin based after adding different ratio from titanium oxide.

Keywords: Alloys, Titanium oxide, Corrosion parameters, Microstructure, Mechanical properties

Introduction

Materials are so significant in the development of civilization. Almost no metals are used in pure form, but they are always combined with each other to recover one or more properties. An alloy may be defined as a substance that has the metallic properties and is composed of two or more chemical elements of which at least one is a metal. Most alloys are great importance in industry and in the arts than are the pure metals. Several researches reported that, modification structure by adding alloying elements to tin or bismuth-based alloys caused minor/ or major effects on measured physical properties such as elastic modulus, hardness, melting temperature, internal friction, spreading, resistivity and electrochemical corrosion behavior with corrosion parameters [1-17]. Microstructure, mechanical and thermal properties of bismuth or tin based alloys are studied [18-23] studied at different conditions. Matrix structure of these alloys is changed which effects on all measured physical properties.

Titanium dioxide (TiO₂)

Titanium and some of its alloys are used as biomaterials for dental and orthopedic applications. Titanium is used in condensers and turbine blades in electric power plants. It is also incorporated into the architecture of buildings, roofs, piping and cable. Titanium dioxide has a wide range of applications, from paint to sunscreen to food coloring. It has eight modifications rutile, anatase, brookite, α -PbO₂-like, baddeleyite like, cotunnite-like, orthorhombic OI and cubic phases) also exist. Titanium Dioxide has high gloss, good whiteness, good discernibility, good liquidity, extraordinary hiding power and good coloring power, good weather resisting property and chalk resistance performance. It has the highest refractive index. Titanium dioxide melts at 1843 °C and its density is 4.23gm/cm³.

Microstructure

$\text{Sn}_{82-x}\text{Bi}_{15}\text{Zn}_3\text{Ti}_x\text{O}_x$ (x= 0.3, 0.6, 0.9 and 1.2) alloys consist of tetragonal β -Sn phase, hexagonal Bi phase, Zn phase with undetected Ti₂O or intermetallic compounds and solid solution from dissolved atoms that changed alloy matrix structure. Adding different ratio (0.5 to 1.5 wt. % at the expense of bismuth) from titanium oxide (TiO₂) to Bi_{50-x}Pb₁₅Sn₂₂Cd₃In₁₀ alloy caused a change in matrix structure such as feature formed phases, crystal size, lattice

distortion, lattice parameters, (a and c), and unit volume cell (V) [9] as listed in Table 1. Scanning electron micrographs, SEM, of $\text{Bi}_{50-x}\text{Pb}_{15}\text{Sn}_{22}\text{In}_{10}\text{Cd}_3(\text{TiO}_2)_x$ ($x=0$ to 1.5 wt.%) alloys show heterogeneous

structure (different feature for formed phases with different grain size beside a solid solution) as shown in Figure 1 which agreed with x-ray analysis.

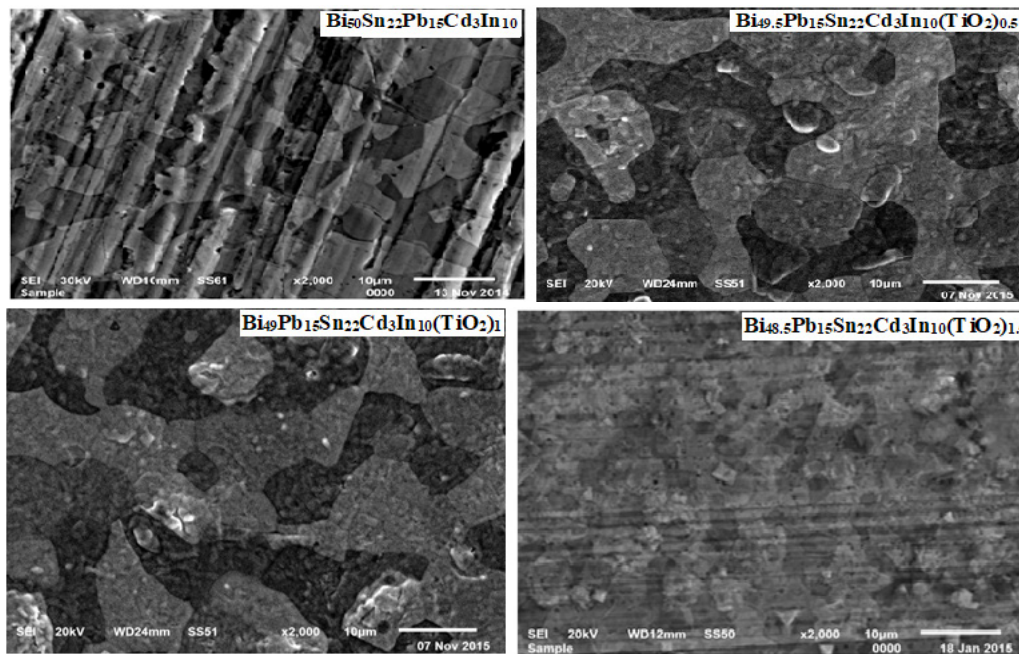


Figure 1: SEM of $\text{Bi}_{50-x}\text{Pb}_{15}\text{Sn}_{22}\text{In}_{10}\text{Cd}_3(\text{TiO}_2)_x$ alloys [9].

Table 1: Crystal size, lattice parameters and lattice distortion of rhombohedral Bi phase [9].

Alloys	Particle size Å	a_{rtho} Å	Lattice Distortion $\times 10^{-3}$
$\text{Bi}_{50}\text{Sn}_{22}\text{Pb}_{15}\text{Cd}_3\text{In}_{10}$	357.64	4.75	1.44
$\text{Bi}_{49.5}\text{Pb}_{15}\text{Sn}_{22}\text{Cd}_3\text{In}_{10}(\text{TiO}_2)_{0.5}$	283.29	4.68	1.43
$\text{Bi}_{49}\text{Pb}_{15}\text{Sn}_{22}\text{Cd}_3\text{In}_{10}(\text{TiO}_2)_1$	356.94	4.68	1.86
$\text{Bi}_{48.5}\text{Pb}_{15}\text{Sn}_{22}\text{Cd}_3\text{In}_{10}(\text{TiO}_2)_{1.5}$	301.45	4.79	1.74

$\text{Sn}_{82-x}\text{Bi}_{15}\text{Zn}_3\text{Ti}_2\text{O}_x$ ($x=0.3, 0.6, 0.9$ and 1.2) alloys consist of tetragonal β -Sn phase, hexagonal Bi phase, Zn phase with undetected Ti_2O or intermetallic compounds and solid solution from dissolved atoms that changed alloy matrix structure. From SEM, Figure 2, adding Ti_2O to $\text{Sn}_{82}\text{Bi}_{15}\text{Zn}_3$ alloy caused a change in its matrix microstructure (quantity, size and orientation of formed phases) [24]. Lattice microstrain, ϵ , determined from draw the relation between full width half maximum, FWHM, and $4\tan\theta$ using Williamson and Hall equation. Lattice microstrain of $\text{Sn}_{82}\text{Bi}_{15}\text{Zn}_3$ alloy increased after adding titanium dioxide as listed in Table 2.

Table 2: Lattice microstrain of $\text{Sn}_{82-x}\text{Bi}_{15}\text{Zn}_3\text{Ti}_2\text{O}_x$ alloys [24].

Alloys	ϵ
$\text{Sn}_{82}\text{Bi}_{15}\text{Zn}_3$	0.011
$\text{Sn}_{81.7}\text{Bi}_{15}\text{Zn}_3(\text{Ti}_2\text{O})_{0.3}$	0.041
$\text{Sn}_{81.4}\text{Bi}_{15}\text{Zn}_3(\text{Ti}_2\text{O})_{0.6}$	0.054

$\text{Sn}_{81.1}\text{Bi}_{15}\text{Zn}_3(\text{Ti}_2\text{O})_{0.9}$	0.021
$\text{Sn}_{80.8}\text{Bi}_{15}\text{Zn}_3(\text{Ti}_2\text{O})_{1.2}$	0.066

$\text{Sn}_{60}\text{Bi}_{30-x}\text{Sb}_6\text{Zn}_4\text{Cu}_{0.7}\text{Ti}_2\text{O}_x$ ($x=0, 0.3, 0.6, 0.9$ and 1.2) alloys consist of tetragonal β -Sn phase, hexagonal Bi phase, Zn phase, undetected phases such as Ti_2O or Sb or Cu or intermetallic compounds and solid solution from dissolved atoms [25]. Lattice microstrain of $\text{Sn}_{60}\text{Bi}_{30-x}\text{Sb}_6\text{Zn}_4\text{Cu}_{0.7}$ alloys varied after adding titanium oxide as listed in Table 3. SEM of $\text{Sn}_{60}\text{Bi}_{30-x}\text{Sb}_6\text{Zn}_4\text{Cu}_{0.7}\text{Ti}_2\text{O}_x$ alloys show heterogeneous structure from formed phases in matrix structure as shown in Figure 3 which agree with x-ray analysis.

Table 3: Lattice microstrain of $\text{Sn}_{60}\text{Bi}_{30-x}\text{Sb}_6\text{Zn}_4\text{Cu}_{0.7}\text{Ti}_2\text{O}_x$ alloys [25].

Alloys	ϵ
$\text{Sn}_{82}\text{Bi}_{15}\text{Zn}_3$	0.12
$\text{Sn}_{81.7}\text{Bi}_{15}\text{Zn}_3(\text{Ti}_2\text{O})_{0.3}$	0.06
$\text{Sn}_{81.4}\text{Bi}_{15}\text{Zn}_3(\text{Ti}_2\text{O})_{0.6}$	0.12
$\text{Sn}_{81.1}\text{Bi}_{15}\text{Zn}_3(\text{Ti}_2\text{O})_{0.9}$	0.1
$\text{Sn}_{80.8}\text{Bi}_{15}\text{Zn}_3(\text{Ti}_2\text{O})_{1.2}$	0.13

The $\text{Sn}_{76}\text{Al}_{10}\text{Bi}_{10-x}\text{Cu}_2\text{Zn}_2(\text{TiO}_2)_x$ ($x=0.5$ to 1.5 wt.%) alloys consist of tetragonal β -Sn phase and hexagonal Bi phase with formed a solid solution or undetected phases. The crystallinity, crystal size and orientations for formed phases of $\text{Sn}_{76}\text{Al}_{10}\text{Bi}_{10}\text{Cu}_2\text{Zn}_2$ alloy changed after adding titanium oxide nanoparticles [26]. The estimated crystal size was given through measured diffraction pattern broadening by Scherer formula. Crystal size of β -Sn phase in $\text{Sn}_{76}\text{Al}_{10}\text{Bi}_{10}\text{Cu}_2\text{Zn}_2$ alloy varied after adding titanium dioxide

as presented in Table 4. Lattice microstrain of $\text{Sn}_{76}\text{Al}_{10}\text{Bi}_{10}\text{Cu}_2\text{Zn}_2$ alloy decreased after adding titanium oxide up to 1wt. % and then increased as listed in Table 4. The $\text{Sn}_{76}\text{Al}_{10}\text{Bi}_9\text{Cu}_2\text{Zn}_2(\text{TiO}_2)_1$ alloy has lower microstrain value. SEM show that adding different ratio from TiO_2 nanoparticles to $\text{Sn}_{76}\text{Al}_{10}\text{Bi}_{10}\text{Cu}_2\text{Zn}_2$ alloy changed the shape

and size of dendrite structure and disturbed dissolved atoms as grains in it as seen in Figure 4. SEM analysis for used alloys shows heterogeneity structure and that is agreed with x-ray analysis [26].

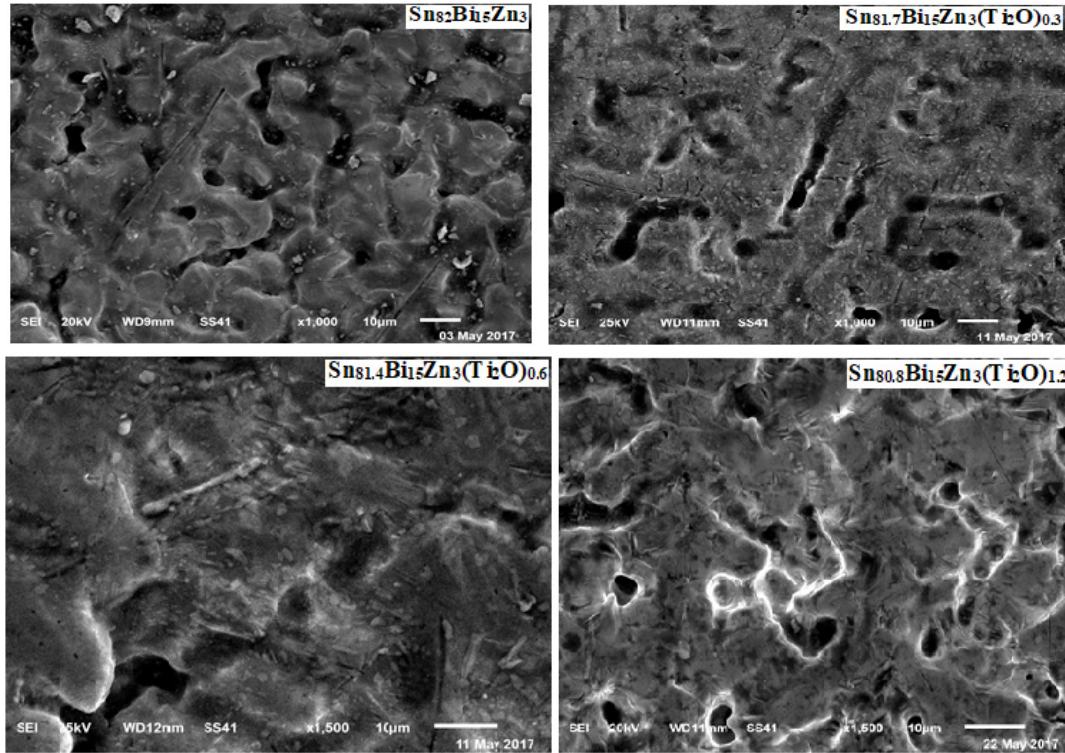


Figure 2: SEM of $\text{Sn}_{82-x}\text{Bi}_{15}\text{Zn}_3\text{Ti}_2\text{O}_x$ alloys [24].

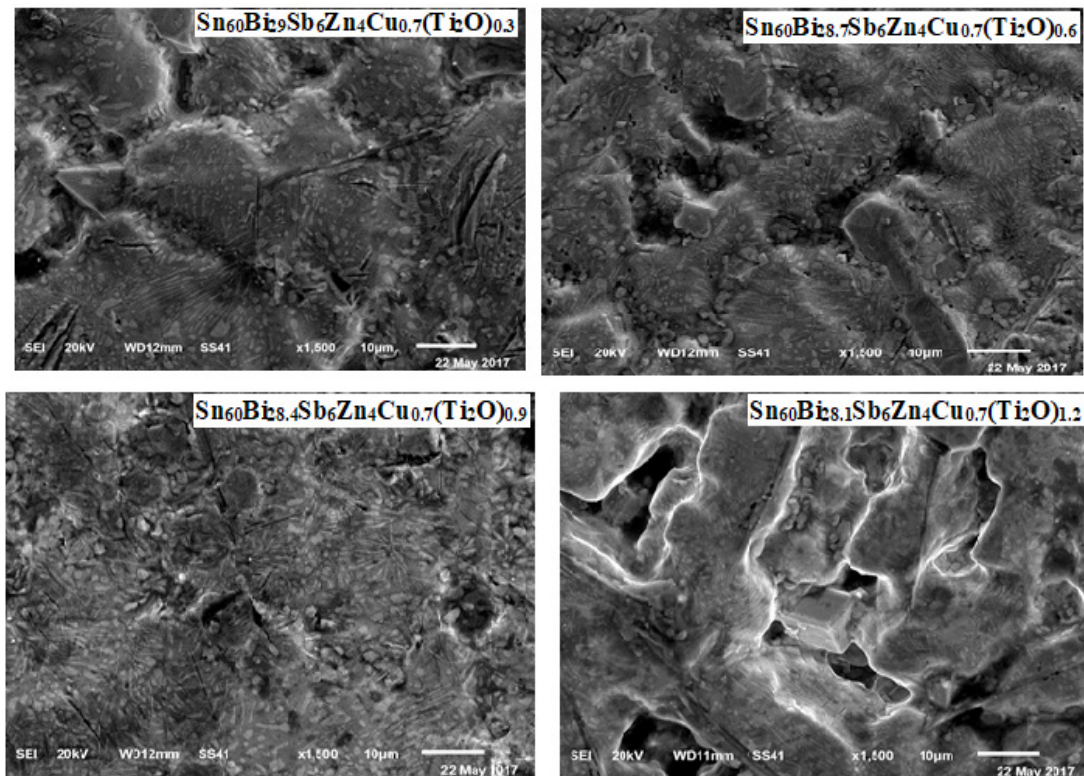


Figure 3: SEM of $\text{Sn}_{60}\text{Bi}_{30-x}\text{Sb}_6\text{Zn}_4\text{Cu}_{0.7}\text{Ti}_2\text{O}_x$ alloys [25].

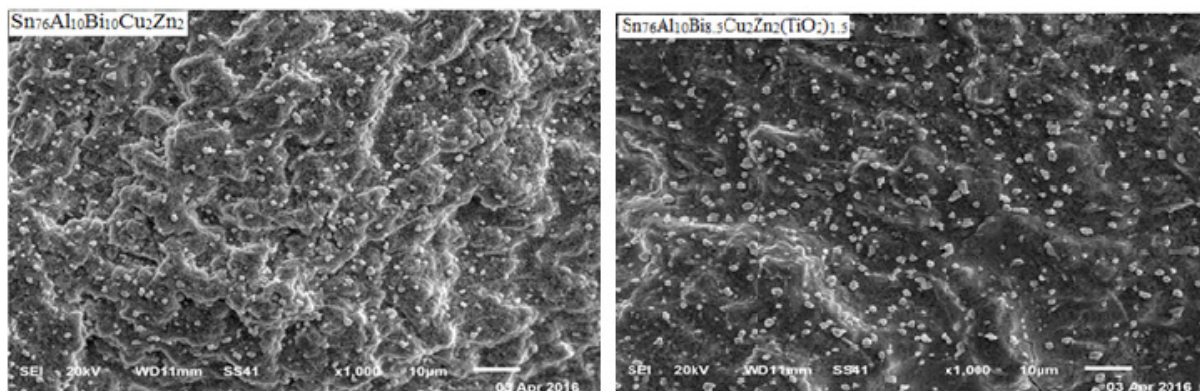


Figure 4: SEM of $\text{Sn}_{76}\text{Al}_{10}\text{Bi}_{10-x}\text{Cu}_2\text{Zn}_2(\text{TiO}_2)_x$ alloys [26].

Table 4: Crystal size of β -Sn and lattice microstrain in $\text{Sn}_{76}\text{Al}_{10}\text{Bi}_{10-x}\text{Cu}_2\text{Zn}_2(\text{TiO}_2)_x$ alloys [26].

Alloys	(Sn) τ (Å)	$\epsilon \times 10^{-3}$
$\text{Sn}_{76}\text{Al}_{10}\text{Bi}_{10}\text{Cu}_2\text{Zn}_2$	347.647	0.9
$\text{Sn}_{76}\text{Al}_{10}\text{Bi}_{9.5}\text{Cu}_2\text{Zn}_2(\text{TiO}_2)_{0.5}$	387.704	0.7
$\text{Sn}_{76}\text{Al}_{10}\text{Bi}_9\text{Cu}_2\text{Zn}_2(\text{TiO}_2)_1$	383.817	0.4
$\text{Sn}_{76}\text{Al}_{10}\text{Bi}_{8.5}\text{Cu}_2\text{Zn}_2(\text{TiO}_2)_{1.5}$	352.74	1.3

$\text{Sn}_{61}\text{Bi}_{25}\text{Sb}_5\text{Zn}_4\text{Al}_{3-x}\text{Ag}_2(\text{TiO}_2)_x$ ($x=0.3$ to 1.2 wt.%) alloys consist of β -Sn phase, hexagonal Bi phase and dissolved Sb, Zn, Al, Ag atoms with TiO_2 nanoparticles or undetected phases in matrix [27]. Crystal size of β -Sn phase in $\text{Sn}_{61}\text{Bi}_{25}\text{Sb}_5\text{Zn}_4\text{Al}_3\text{Ag}_2$ alloy varied after adding TiO_2 nanoparticles as listed in Table 5. $\text{Sn}_{61}\text{Bi}_{25}\text{Sb}_5\text{Zn}_4\text{Al}_{2.4}\text{Ag}_2(\text{TiO}_2)_{0.6}$ alloy has higher lattice microstrain and lower β -Sn phase crystal size. SEM of $\text{Sn}_{61}\text{Bi}_{25}\text{Sb}_5\text{Zn}_4\text{Al}_{3-x}\text{Ag}_2(\text{TiO}_2)_x$ alloys [27], Figure 5, show that the matrix structure of $\text{Sn}_{61}\text{Bi}_{25}\text{Sb}_5\text{Zn}_4\text{Al}_3\text{Ag}_2$ alloy changed after adding TiO_2 which agree with x-ray analysis and affected all measured properties.

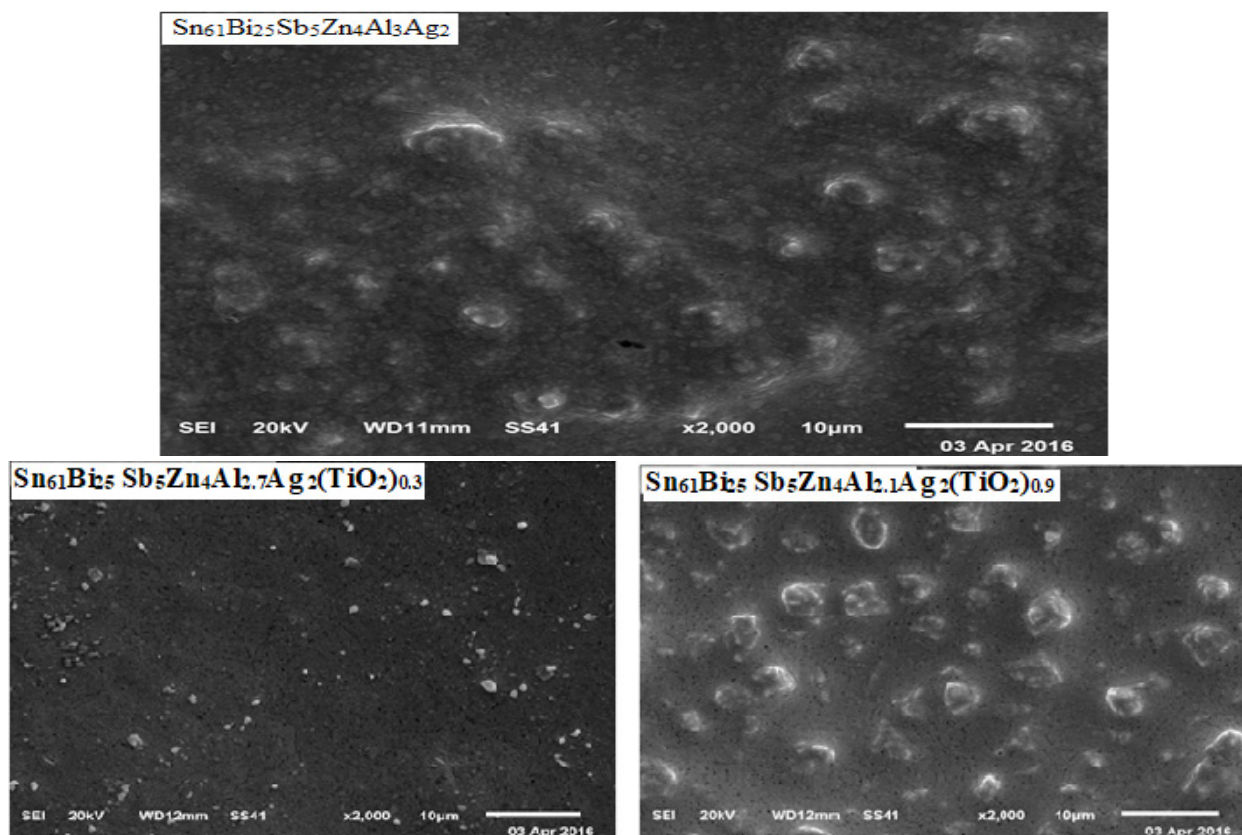


Figure 5: SEM of $\text{Sn}_{61}\text{Bi}_{25}\text{Sb}_5\text{Zn}_4\text{Al}_{3-x}\text{Ag}_2(\text{TiO}_2)_x$ alloys [27].

$\text{Sn}_{80}\text{Sb}_{15}\text{Pb}_5$ alloy consists of β -Sn and SbSn intermetallic phases. After adding different ratio of titanium oxide (TiO_2) nanoparticles to $\text{Sn}_{80}\text{Sb}_{15}\text{Pb}_5$ alloy, SbSn intermetallic phase disappeared with

changing matrix microstructure [28]. Lattice parameters, (a and c), unit volume cell (V) and crystal size (τ) of β -Sn phase in $\text{Sn}_{80-x}\text{Sb}_{15}\text{Pb}_5(\text{TiO}_2)_x$ ($x=0, 0.5, 1$ and 1.5 wt. %) alloys are determined

and then recorded in Table 6. Little variation occurred in lattice parameters and unit volume of β -Sn in $\text{Sn}_{80-x}\text{Sb}_{15}\text{Pb}_5(\text{TiO}_2)_x$ alloys but a major variation in β -Sn crystal size after adding titanium oxide nanoparticles. Scanning electron micrographs, SEM, of $\text{Sn}_{80}\text{Sb}_{15}\text{Pb}_5$ and $\text{Sn}_{78.5}\text{Sb}_{15}\text{Pb}_5(\text{TiO}_2)_{1.5}$ alloys show heterogeneous structure as shown in Figure 6 and that agreed with x-ray analysis. Adding TiO_2 caused a change in matrix microstructure of $\text{Sn}_{80}\text{Sb}_{15}\text{Pb}_5$ alloy.

Table 5: Crystal size of β -Sn and lattice microstrain in $\text{Sn}_{61}\text{Bi}_{25}\text{Sb}_5\text{Zn}_4\text{Al}_{3-x}\text{Ag}_2(\text{TiO}_2)_x$ alloys [27].

Alloys	(Sn) τ (Å)	$\epsilon \times 10^{-3}$
$\text{Sn}_{61}\text{Bi}_{25}\text{Sb}_5\text{Zn}_4\text{Al}_3\text{Ag}_2$	465.93	0.4
$\text{Sn}_{61}\text{Bi}_{25}\text{Sb}_5\text{Zn}_4\text{Al}_{2.7}\text{Ag}_2(\text{TiO}_2)_{0.3}$	522.97	0.4

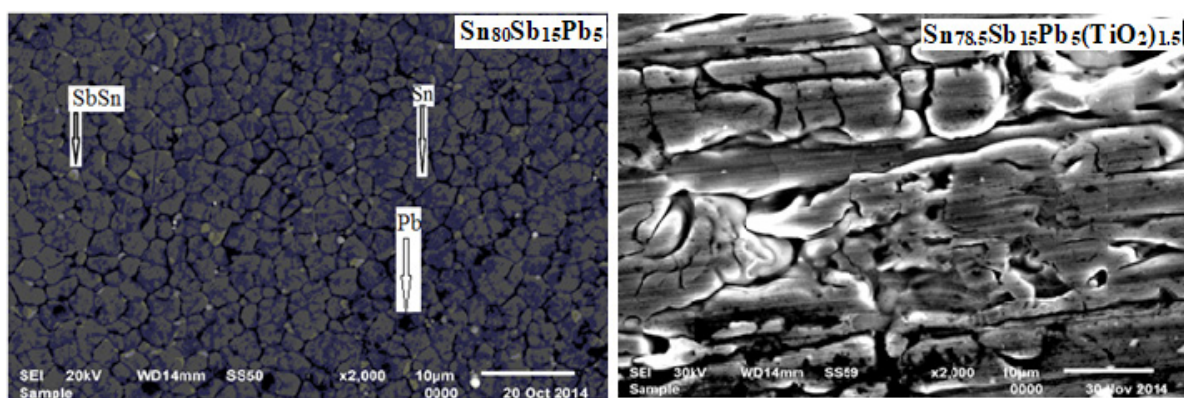


Figure 6: SEM of $\text{Sn}_{80-x}\text{Sb}_{15}\text{Pb}_5(\text{TiO}_2)_x$ alloys [28].

$\text{Sn}_{60-x}\text{Al}_{20}\text{Sb}_{15}\text{Pb}_5(\text{TiO}_2)_x$ ($x = 0.5, 1$ and 1.5 wt.%) alloys consist of β -Sn, Pb and SbSn intermetallic phases [28]. The determined lattice parameters, unit volume cell and crystal size of β -Sn phase in $\text{Sn}_{60-x}\text{Al}_{20}\text{Sb}_{15}\text{Pb}_5(\text{TiO}_2)_x$ recorded in Table 7. A little variation happened in lattice parameters and unit volume of β -Sn in $\text{Sn}_{80-x}\text{Sb}_{15}\text{Pb}_5(\text{TiO}_2)_x$ alloys after adding titanium oxide nanoparticles but a major variation occurred in β -Sn crystal size. That is because

TiO_2 nanoparticles dissolved in matrix alloy formed a solid solution and resultant in disappeared or appeared phases with changed the shape of rest phases. Dissimilar structure for $\text{Sn}_{60}\text{Sb}_{15}\text{Pb}_5\text{Al}_{20}$ and $\text{Sn}_{58.5}\text{Sb}_{15}\text{Pb}_5\text{Al}_{20}(\text{TiO}_2)_{1.5}$ alloys are shown in scanning electron micrographs, Figure 7, which agreed with x-ray analysis. That is meant adding TiO_2 caused a change in matrix microstructure [28].

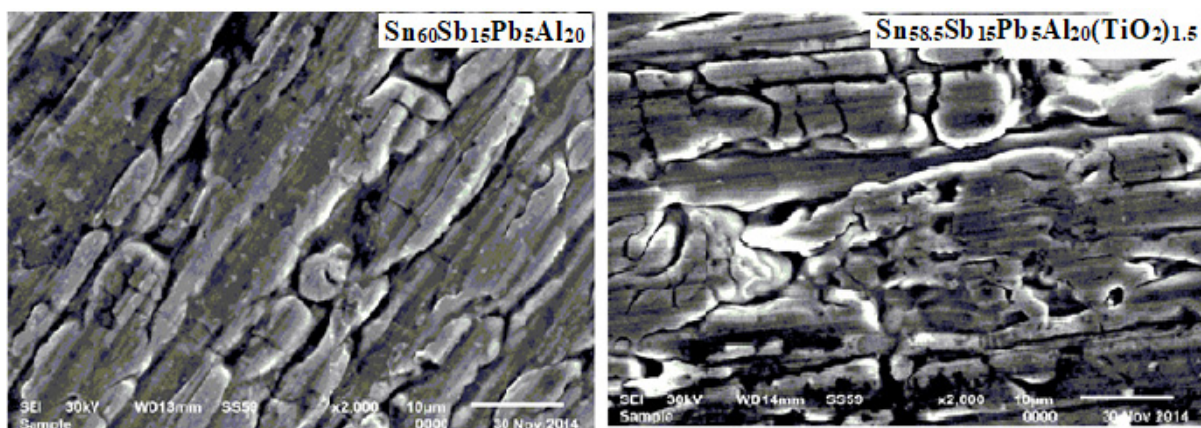


Figure 7: SEM of $\text{Sn}_{60-x}\text{Al}_{20}\text{Sb}_{15}\text{Pb}_5(\text{TiO}_2)_x$ alloys [28].

$\text{Sn}_{645-x}\text{Ag}_{3.5}\text{Bi}_{30}\text{In}_2(\text{TiO}_2)_x$ ($x = 0.5, 1$ and 1.5 wt. %) alloys consist of β -Sn, Ag_3Sn and hexagonal Bi phases [29]. That is meant that in atoms and TiO_2 nanoparticles dissolved in alloy matrix

forming a solid solution with changing microstructure. Lattice parameters, unit volume cell and crystal size of β -Sn in $\text{Sn}_{645-x}\text{Ag}_{3.5}\text{Bi}_{30}\text{In}_2(\text{TiO}_2)_x$ alloys are determined and then presented in

$\text{Sn}_{61}\text{Bi}_{25}\text{Sb}_5\text{Zn}_4\text{Al}_{2.4}\text{Ag}_2(\text{TiO}_2)_{0.6}$	300.46	2.3
$\text{Sn}_{61}\text{Bi}_{25}\text{Sb}_5\text{Zn}_4\text{Al}_{2.1}\text{Ag}_2(\text{TiO}_2)_{0.9}$	611	0.8
$\text{Bi}_{25}\text{Sn}_{61}\text{Sb}_5\text{Zn}_4\text{Al}_{1.8}\text{Ag}_2(\text{TiO}_2)_{1.2}$	692.52	0.5
$\text{Bi}_{25}\text{Sn}_{61}\text{Sb}_5\text{Zn}_4\text{Al}_{1.5}\text{Ag}_2(\text{TiO}_2)_{1.5}$	388.4	1.8

Table 6: Matrix parameters (a, b, c, V and τ) of $\text{Sn}_{80-x}\text{Sb}_{15}\text{Pb}_5(\text{TiO}_2)_x$ alloys [28].

Alloys	a Å	b Å	c Å	V Å ³	τ (Å)
$\text{Sn}_{80}\text{Sb}_{15}\text{Pb}_5$	5.854	3.184	0.543	109.144	317.25
$\text{Sn}_{79.5}\text{Sb}_{15}\text{Pb}_5(\text{TiO}_2)_{0.5}$	5.84	3.188	0.545	108.88	395.12
$\text{Sn}_{79}\text{Sb}_{15}\text{Pb}_5(\text{TiO}_2)_1$	5.84	3.180	0.544	108.77	448.06
$\text{Sn}_{78.5}\text{Sb}_{15}\text{Pb}_5(\text{TiO}_2)_{1.5}$	5.84	3.188	0.545	108.65	415.38

Table 8. Unit cell volume of β -Sn in $\text{Sn}_{64.5-x}\text{Ag}_{3.5}\text{Bi}_{30}\text{In}_2(\text{TiO}_2)_x$ alloys decreased but lattice parameter, a, and crystal size varied after adding TiO_2 nanoparticles. The internal lattice microstrain of $\text{Sn}_{64.5-x}\text{Ag}_{3.5}\text{Bi}_{30}\text{In}_2(\text{TiO}_2)_x$ alloys also was determined then show in Table 8. Lattice strain of $\text{Sn}_{64.5-x}\text{Ag}_{3.5}\text{Bi}_{30}\text{In}_2(\text{TiO}_2)_x$ increased with increasing TiO_2 nanoparticles ratio.

Table 7: Matrix parameters (a, b, c, V and τ) of $\text{Sn}_{60-x}\text{Al}_{20}\text{Sb}_{15}\text{Pb}_5(\text{TiO}_2)_x$ alloys [28].

Alloys	a Å	c Å	c Å	V Å ³	τ (Å)
$\text{Sn}_{60}\text{Sb}_{15}\text{Pb}_5\text{Al}_{20}$	5.85	3.189	0.545	109.29	337.70
$\text{Sn}_{59.5}\text{Sb}_{15}\text{Pb}_5\text{Al}_{20}(\text{TiO}_2)_{0.5}$	5.85	3.187	0.544	108.97	412.47
$\text{Sn}_{59}\text{Sb}_{15}\text{Pb}_5\text{Al}_{20}(\text{TiO}_2)_1$	5.85	3.186	0.544	108.96	409.78
$\text{Sn}_{58.5}\text{Sb}_{15}\text{Pb}_5\text{Al}_{20}(\text{TiO}_2)_{1.5}$	5.85	3.188	0.544	109.15	368.36

Table 8: Matrix parameters (a, c, V, τ and ϵ) of $\text{Sn}_{64.5-x}\text{Ag}_{3.5}\text{Bi}_{30}\text{In}_2(\text{TiO}_2)_x$ alloys [29].

Alloys	a Å	c Å	V Å ³	τ (Å)	$\epsilon \times 10^{-4}$
$\text{Sn}_{64.5}\text{Ag}_{3.5}\text{Bi}_{30}\text{In}_2$	5.851	3.29	112.622	300.19	2
$\text{Sn}_{64}\text{Ag}_{3.5}\text{Bi}_{30}\text{In}_2(\text{TiO}_2)_{0.5}$	5.856	3.196	109.599	261.516	7
$\text{Sn}_{63.5}\text{Ag}_{3.5}\text{Bi}_{30}\text{In}_2(\text{TiO}_2)_1$	5.851	3.1927	109.288	293.482	5
$\text{Sn}_{63}\text{Ag}_{3.5}\text{Bi}_{30}\text{In}_2(\text{TiO}_2)_{1.5}$	5.857	3.1911	109.468	311.438	6

$\text{Sn}_{87-x}\text{Sb}_{10}\text{Pb}_3(\text{TiO}_2)_x$ ($x=0.5, 1$ and 1.5 wt. %) alloys consist of β -Sn, Pb/or Sb and SbSn intermetallic phases [30]. Adding TiO_2 to $\text{Sn}_{87}\text{Sb}_{10}\text{Pb}_3$ alloy caused a change in Sn matrix structure such as lattice parameters and formed crystal structure (crystallinity, crystal size and the orientation) as seen in Table 9. That is because TiO_2 nanoparticles dissolved in Sn matrix formed a solid solution and other accumulated particles formed a trace of phases. Also $\text{Sn}_{80-x}\text{Al}_{20}(\text{TiO}_2)_x$ ($x=0.5, 1$ and 1.5 wt.%) alloys consist of β -Sn and Al phases [31]. Adding TiO_2 to $\text{Sn}_{80}\text{Al}_{20}$ alloy caused a change in Sn matrix such as lattice parameters and formed crystal structure (crystallinity and crystal size) as seen in Table 10.

Table 9: Matrix parameters (a, c, V and τ) of $\text{Sn}_{64.5-x}\text{Ag}_{3.5}\text{Bi}_{30}\text{In}_2(\text{TiO}_2)_x$ alloys [30].

Alloys	a Å	c Å	V Å ³	τ (Å)
$\text{Sn}_{87}\text{Sb}_{10}\text{Pb}_3$	5.857	3.17	108.88	355.44
$\text{Sn}_{86.5}\text{Sb}_{10}\text{Pb}_3(\text{TiO}_2)_{0.5}$	5.841	3.18	108.62	514.28
$\text{Sn}_{86}\text{Sb}_{10}\text{Pb}_3(\text{TiO}_2)_1$	5.841	3.2	109.15	508.04
$\text{Sn}_{85.5}\text{Sb}_{10}\text{Pb}_3(\text{TiO}_2)_{1.5}$	5.843	3.19	108.83	529.68

Table 10: Matrix parameters (a, c, V and τ) of $\text{Sn}_{80-x}\text{Al}_{20}(\text{TiO}_2)_x$ alloys [30].

Alloys	a Å	c Å	V Å ³	τ (Å)
$\text{Sn}_{80}\text{Al}_{20}$	5.84	3.19	108.65	461.64
$\text{Sn}_{79.5}\text{Al}_{20}(\text{TiO}_2)_{0.5}$	5.88	3.10	106.42	390.49
$\text{Sn}_{79}\text{Al}_{20}(\text{TiO}_2)_1$	5.84	3.16	107.69	689.28
$\text{Sn}_{78.5}\text{Al}_{20}(\text{TiO}_2)_{1.5}$	5.84	3.17	108.08	

Thermal properties

Measurement of thermal parameters is very inertial for their applications, particularly in the construction of devices. The melting temperature value of $\text{Bi}_{50-x}\text{Pb}_{15}\text{Sn}_{22}\text{In}_{10}\text{Cd}_3(\text{TiO}_2)_x$ alloys increased after adding TiO_2 nanoparticles which dependent on alloy compositions or alloy structure as presented in Table 11. The melting temperature value of $\text{Sn}_{82}\text{Bi}_{15}\text{Zn}_3$ alloy is decreased after adding different ratio from titanium oxide as listed in Table 12. The melting temperature value of $\text{Sn}_{60}\text{Bi}_{29}\text{Sb}_6\text{Zn}_4\text{Cu}_{0.7}$ alloy is varied after adding different ratio from titanium oxide as shown in Table 13. But no significant effect on melting temperature value of $\text{Sn}_{76}\text{Al}_{10}\text{Bi}_{10}\text{Cu}_2\text{Zn}_2$ alloy after adding titanium dioxide nanoparticles as presented in Table 14.

Table 11: Melting temperature of $\text{Bi}_{50-x}\text{Pb}_{15}\text{Sn}_{22}\text{In}_{10}\text{Cd}_3(\text{TiO}_2)_x$ alloys [9].

Alloys	Melting Temperature °C
$\text{Bi}_{50}\text{Sn}_{22}\text{Pb}_{15}\text{Cd}_3\text{In}_{10}$	58.22
$\text{Bi}_{49.5}\text{Pb}_{15}\text{Sn}_{22}\text{Cd}_3\text{In}_{10}(\text{TiO}_2)_{0.5}$	68.84
$\text{Bi}_{49}\text{Pb}_{15}\text{Sn}_{22}\text{Cd}_3\text{In}_{10}(\text{TiO}_2)_1$	91.37
$\text{Bi}_{48.5}\text{Pb}_{15}\text{Sn}_{22}\text{Cd}_3\text{In}_{10}(\text{TiO}_2)_{1.5}$	109.63

Table 12: Melting temperature of $\text{Sn}_{82-x}\text{Bi}_{15}\text{Zn}_3\text{Ti}_2\text{O}_x$ alloys [24].

Alloys	Melting Temperature °C
$\text{Sn}_{82}\text{Bi}_{15}\text{Zn}_3$	216.42
$\text{Sn}_{81.7}\text{Bi}_{15}\text{Zn}_3(\text{Ti}_2\text{O})_{0.3}$	212
$\text{Sn}_{81.4}\text{Bi}_{15}\text{Zn}_3(\text{Ti}_2\text{O})_{0.6}$	210.7
$\text{Sn}_{81.1}\text{Bi}_{15}\text{Zn}_3(\text{Ti}_2\text{O})_{0.9}$	187.11
$\text{Sn}_{80.8}\text{Bi}_{15}\text{Zn}_3(\text{Ti}_2\text{O})_{1.2}$	187.3

Table 13: Melting temperature of $\text{Sn}_{60}\text{Bi}_{30-x}\text{Sb}_6\text{Zn}_4\text{Cu}_{0.7}(\text{Ti}_2\text{O})_x$ alloys [25].

Alloys	Melting Temperature °C
$\text{Sn}_{60}\text{Bi}_{29}\text{Sb}_6\text{Zn}_4\text{Cu}_{0.7}(\text{Ti}_2\text{O})_{0.3}$	187.3
$\text{Sn}_{60}\text{Bi}_{28.7}\text{Sb}_6\text{Zn}_4\text{Cu}_{0.7}(\text{Ti}_2\text{O})_{0.6}$	180.85
$\text{Sn}_{60}\text{Bi}_{28.4}\text{Sb}_6\text{Zn}_4\text{Cu}_{0.7}(\text{Ti}_2\text{O})_{0.9}$	183.26
$\text{Sn}_{60}\text{Bi}_{28.1}\text{Sb}_6\text{Zn}_4\text{Cu}_{0.7}(\text{Ti}_2\text{O})_{1.2}$	175.21

Table 14: Melting temperature of $\text{Sn}_{76}\text{Al}_{10}\text{Bi}_{10-x}\text{Cu}_2\text{Zn}_2(\text{TiO}_2)_x$ alloys [26].

Alloys	Melting Temperature °C
$\text{Sn}_{76}\text{Al}_{10}\text{Bi}_{10}\text{Cu}_2\text{Zn}_2$	212
$\text{Sn}_{76}\text{Al}_{10}\text{Bi}_{9.5}\text{Cu}_2\text{Zn}_2(\text{TiO}_2)_{0.5}$	210.1
$\text{Sn}_{76}\text{Al}_{10}\text{Bi}_9\text{Cu}_2\text{Zn}_2(\text{TiO}_2)_1$	212.3
$\text{Sn}_{76}\text{Al}_{10}\text{Bi}_{8.5}\text{Cu}_2\text{Zn}_2(\text{TiO}_2)_{1.5}$	213.8

Melting temperature of $\text{Sn}_{61}\text{Bi}_{25}\text{Sb}_5\text{Zn}_4\text{Al}_3\text{Ag}_2$ alloy varied after adding TiO_2 nanoparticles as listed in Table 15. It is increased up to 0.9 wt. % TiO_2 nanoparticles and then it's decreased. Melting temperature of $\text{Sn}_{80}\text{Sb}_{10}\text{Pb}_5$ alloy decreased after adding TiO_2 nanoparticles as presented in Table 16. Melting temperature of $\text{Sn}_{60}\text{Al}_{20}\text{Sb}_{15}\text{Pb}_5$ alloy varied after adding TiO_2 nanoparticles as

presented in Table 17. That is because TiO_2 nanoparticles due a change in matrix microstructure of $\text{Sn}_{60}\text{Al}_{20}\text{Sb}_{15}\text{Pb}_5$ alloy. But melting temperature of $\text{Sn}_{64.5-x}\text{Ag}_{3.5}\text{Bi}_{30}\text{In}_2(\text{TiO}_2)_x$ ($x=0.5, 1$ and 1.5 wt. %) alloys varied after adding TiO_2 nanoparticles as listed in Table 18.

Table 15: Melting temperature of $\text{Sn}_{61}\text{Bi}_{25}\text{Sb}_5\text{Zn}_4\text{Al}_3\text{Ag}_2(\text{TiO}_2)_x$ alloys [27].

Alloys	Melting Temperature °C
$\text{Sn}_{61}\text{Bi}_{25}\text{Sb}_5\text{Zn}_4\text{Al}_3\text{Ag}_2$	167.7
$\text{Sn}_{61}\text{Bi}_{25}\text{Sb}_5\text{Zn}_4\text{Al}_{2.7}\text{Ag}_2(\text{TiO}_2)_{0.3}$	174.1
$\text{Sn}_{61}\text{Bi}_{25}\text{Sb}_5\text{Zn}_4\text{Al}_{2.4}\text{Ag}_2(\text{TiO}_2)_{0.6}$	187.5
$\text{Sn}_{61}\text{Bi}_{25}\text{Sb}_5\text{Zn}_4\text{Al}_{2.1}\text{Ag}_2(\text{TiO}_2)_{0.9}$	189.1
$\text{Bi}_{25}\text{Sn}_{61}\text{Sb}_5\text{Zn}_4\text{Al}_{1.8}\text{Ag}_2(\text{TiO}_2)_{1.2}$	173.5
$\text{Bi}_{25}\text{Sn}_{61}\text{Sb}_5\text{Zn}_4\text{Al}_{1.5}\text{Ag}_2(\text{TiO}_2)_{1.5}$	170.1

Table 16: Melting temperature of $\text{Sn}_{80-x}\text{Sb}_{15}\text{Pb}_5(\text{TiO}_2)_x$ alloys [28].

Alloys	Melting Temperature °C
$\text{Sn}_{80}\text{Sb}_{15}\text{Pb}_5$	231.23
$\text{Sn}_{79.5}\text{Sb}_{15}\text{Pb}_5(\text{TiO}_2)_{0.5}$	228.03
$\text{Sn}_{79}\text{Sb}_{15}\text{Pb}_5(\text{TiO}_2)_1$	225.61
$\text{Sn}_{78.5}\text{Sb}_{15}\text{Pb}_5(\text{TiO}_2)_{1.5}$	227.45

Table 17: Melting temperature of $\text{Sn}_{60-x}\text{Al}_{20}\text{Sb}_{15}\text{Pb}_5(\text{TiO}_2)_x$ alloys [28].

Alloys	Melting Temperature °C
$\text{Sn}_{60}\text{Al}_{20}\text{Sb}_{15}\text{Pb}_5$	229
$\text{Sn}_{59.5}\text{Al}_{20}\text{Sb}_{15}\text{Pb}_5(\text{TiO}_2)_{0.5}$	231.27
$\text{Sn}_{59}\text{Al}_{20}\text{Sb}_{15}\text{Pb}_5(\text{TiO}_2)_1$	224.16
$\text{Sn}_{58.5}\text{Al}_{20}\text{Sb}_{15}\text{Pb}_5(\text{TiO}_2)_{1.5}$	230.94

Table 18: Melting temperature of $\text{Sn}_{64.5-x}\text{Ag}_{3.5}\text{Bi}_{30}\text{In}_2(\text{TiO}_2)_x$ alloys [29].

Alloys	Melting Temperature °C
$\text{Sn}_{64.5}\text{Ag}_{3.5}\text{Bi}_{30}\text{In}_2$	174.12
$\text{Sn}_{64}\text{Ag}_{3.5}\text{Bi}_{30}\text{In}_2(\text{TiO}_2)_{0.5}$	169.67
$\text{Sn}_{63.5}\text{Ag}_{3.5}\text{Bi}_{30}\text{In}_2(\text{TiO}_2)_1$	175.94
$\text{Sn}_{63}\text{Ag}_{3.5}\text{Bi}_{30}\text{In}_2(\text{TiO}_2)_{1.5}$	174.2

Melting temperature of $\text{Sn}_{87}\text{Sb}_{10}\text{Pb}_3$ alloy decreased after adding TiO_2 nanoparticles as shown in Table 19. The melting temperature of $\text{Sn}_{80-x}\text{Al}_{20}(\text{TiO}_2)_x$ ($x= 0.5$ to 1.5 wt.%) alloys are listed in Table 20. Little increased in melting temperature of $\text{Sn}_{80}\text{Al}_{20}$ alloy after adding TiO_2 nanoparticles.

Table 19: Melting temperature of $\text{Sn}_{64.5-x}\text{Ag}_{3.5}\text{Bi}_{30}\text{In}_2(\text{TiO}_2)_x$ alloys [31].

Alloys	Melting Temperature °C
$\text{Sn}_{87}\text{Sb}_{10}\text{Pb}_3$	236.87
$\text{Sn}_{86.5}\text{Sb}_{10}\text{Pb}_3(\text{TiO}_2)_{0.5}$	223.38
$\text{Sn}_{86}\text{Sb}_{10}\text{Pb}_3(\text{TiO}_2)_1$	229.52
$\text{Sn}_{85.5}\text{Sb}_{10}\text{Pb}_3(\text{TiO}_2)_{1.5}$	229.33

Table 20: Melting temperature of $\text{Sn}_{80-x}\text{Al}_{20}(\text{TiO}_2)_x$ alloys [30].

Alloys	Melting Temperature °C
$\text{Sn}_{80}\text{Al}_{20}$	227.03
$\text{Sn}_{79.5}\text{Al}_{20}(\text{TiO}_2)_{0.5}$	228.22
$\text{Sn}_{79}\text{Al}_{20}(\text{TiO}_2)_1$	228.92
$\text{Sn}_{78.5}\text{Al}_{20}(\text{TiO}_2)_{1.5}$	

Mechanical properties

A significant change in elastic modulus of $\text{Bi}_{50-x}\text{Pb}_{15}\text{Sn}_{22}\text{Cd}_3\text{In}_{10}(\text{TiO}_2)_x$ ($x=0.5$ to 1.5 wt.%) alloys with adding different ratio from TiO_2 nanoparticles. Vickers hardness and calculated maximum shear stress of $\text{Bi}_{50}\text{Pb}_{15}\text{Sn}_{22}\text{Cd}_3\text{In}_{10}$ alloy increased after adding (TiO_2) as listed in Table 21.

Table 21: Elastic modulus, hardness and maximum shear stress of $\text{Bi}_{50-x}\text{Pb}_{15}\text{Sn}_{22}\text{In}_{10}\text{Cd}_3(\text{TiO}_2)_x$ alloys [9].

Alloys	E GPa	H_v Kg/mm ²	μ_n Kg/mm ²
$\text{Bi}_{50}\text{Sn}_{22}\text{Pb}_{15}\text{Cd}_3\text{In}_{10}$	29.3	9.72	3.21
$\text{Bi}_{49.5}\text{Pb}_{15}\text{Sn}_{22}\text{Cd}_3\text{In}_{10}(\text{TiO}_2)_{0.5}$	32.03	14.5	4.79
$\text{Bi}_{49}\text{Pb}_{15}\text{Sn}_{22}\text{Cd}_3\text{In}_{10}(\text{TiO}_2)_1$	36.16	19.05	6.27
$\text{Bi}_{48.5}\text{Pb}_{15}\text{Sn}_{22}\text{Cd}_3\text{In}_{10}(\text{TiO}_2)_{1.5}$	23.77	16.6	5.48

Vickers hardness and calculated maximum shear stress of $\text{Sn}_{76}\text{Al}_{10}\text{Bi}_{10-x}\text{Cu}_2\text{Zn}_2(\text{TiO}_2)_x$ alloys at 10 gram force and indentation time 5 sec are presented in Table 22. Vickers hardness value of $\text{Sn}_{76}\text{Al}_{10}\text{Bi}_{10}\text{Cu}_2\text{Zn}_2$ alloy varied after adding titanium oxide nanoparticles.

Table 22: Vickers hardness and maximum shear stress of $\text{Sn}_{76}\text{Al}_{10}\text{Bi}_{10-x}\text{Cu}_2\text{Zn}_2(\text{TiO}_2)_x$ alloys [26].

Alloys	H_v Kg/mm ²	μ_n Kg/mm ²
$\text{Sn}_{76}\text{Al}_{10}\text{Bi}_{10}\text{Cu}_2\text{Zn}_2$	46.6	15.38
$\text{Sn}_{76}\text{Al}_{10}\text{Bi}_{9.5}\text{Cu}_2\text{Zn}_2(\text{TiO}_2)_{0.5}$	24.4	8.05
$\text{Sn}_{76}\text{Al}_{10}\text{Bi}_9\text{Cu}_2\text{Zn}_2(\text{TiO}_2)_1$	39.43	13.013
$\text{Sn}_{76}\text{Al}_{10}\text{Bi}_{8.5}\text{Cu}_2\text{Zn}_2(\text{TiO}_2)_{1.5}$	42.2	13.93

Table 23: Elastic modulus of $\text{Sn}_{80-x}\text{Sb}_{15}\text{Pb}_5(\text{TiO}_2)_x$ alloys [28].

Alloys	E GPa
$\text{Sn}_{80}\text{Sb}_{15}\text{Pb}_5$	24.28
$\text{Sn}_{79.5}\text{Sb}_{15}\text{Pb}_5(\text{TiO}_2)_{0.5}$	32.96
$\text{Sn}_{79}\text{Sb}_{15}\text{Pb}_5(\text{TiO}_2)_1$	38.25
$\text{Sn}_{78.5}\text{Sb}_{15}\text{Pb}_5(\text{TiO}_2)_{1.5}$	42.67

Elastic modulus value of $\text{Sn}_{80-x}\text{Sb}_{15}\text{Pb}_5(\text{TiO}_2)_x$ ($x= 0, 0.5, 1$ and 1.5 wt. %) alloys is listed in Table 23. Elastic modulus of $\text{Sn}_{80}\text{Sb}_{15}\text{Pb}_5$ alloy increased after adding TiO_2 nanoparticles because it's dissolved in alloy matrix. The stress exponent values of $\text{Sn}_{80-x}\text{Sb}_{15}\text{Pb}_5(\text{TiO}_2)_x$ alloys which calculated using Mulheam-Tabor method are given in Table 24. These exponent values are in the range of 2.16 to 3.07 depending on the composition of alloy and that agreed with the previous results [31,32]. The change in stress exponent values are

attributable to microstructural features (such as change in lattice parameters, solid solution, size and distribution of strengthening phases, intermetallic phases) and that is agree with the pervious results [33].

Table 24: Stress exponent (n) of $\text{Sn}_{80-x}\text{Sb}_{15}\text{Pb}_5(\text{TiO}_2)_x$ alloys [28].

Alloys	Stress Exponent (n)
$\text{Sn}_{80}\text{Sb}_{15}\text{Pb}_5$	3.077
$\text{Sn}_{78.5}\text{Sb}_{15}\text{Pb}_5(\text{TiO}_2)_{1.5}$	2.16

Elastic modulus of $\text{Sn}_{60-x}\text{Al}_{20}\text{Sb}_{15}\text{Pb}_5(\text{TiO}_2)_x$ ($x=0.5, 1$ and 1.5 wt.%) alloys are registered in Table 25. Elastic modulus of $\text{Sn}_{60}\text{Al}_{20}\text{Sb}_{15}\text{Pb}_5$ alloy varied after adding TiO_2 nanoparticles. The stress exponent $\text{Sn}_{60}\text{Al}_{20}\text{Sb}_{15}\text{Pb}_5$ alloy decreased after adding TiO_2 nanoparticles as shown in Table 26. These exponent values are in the range of 2.44 to 5.75 depending on the composition of used alloy. Elastic modulus and Vickers hardness values of $\text{Sn}_{64.5}\text{Ag}_{3.5}\text{Bi}_{30}\text{In}_2$ alloy decreased after adding TiO_2 nanoparticles as shown in Table 27.

Table 25: Elastic modulus of $\text{Sn}_{60-x}\text{Al}_{20}\text{Sb}_{15}\text{Pb}_5(\text{TiO}_2)_x$ alloys [28].

Alloys	E GPa
$\text{Sn}_{60}\text{Al}_{20}\text{Sb}_{15}\text{Pb}_5$	38.95
$\text{Sn}_{59.5}\text{Al}_{20}\text{Sb}_{15}\text{Pb}_5(\text{TiO}_2)_{0.5}$	36.99
$\text{Sn}_{59}\text{Al}_{20}\text{Sb}_{15}\text{Pb}_5(\text{TiO}_2)_1$	42.22
$\text{Sn}_{58.5}\text{Al}_{20}\text{Sb}_{15}\text{Pb}_5(\text{TiO}_2)_{1.5}$	37.55

Table 26: Stress exponent (n) of $\text{Sn}_{60-x}\text{Al}_{20}\text{Sb}_{15}\text{Pb}_5(\text{TiO}_2)_x$ alloys [29].

Alloys	Stress Exponent (n)
$\text{Sn}_{60}\text{Al}_{20}\text{Sb}_{15}\text{Pb}_5$	5.749
$\text{Sn}_{58.5}\text{Al}_{20}\text{Sb}_{15}\text{Pb}_5(\text{TiO}_2)_{1.5}$	2.44

Table 27: Elastic modulus and Vickers hardness of $\text{Sn}_{64.5-x}\text{Ag}_{3.5}\text{Bi}_{30}\text{In}_2(\text{TiO}_2)_x$ alloys [29].

Alloys	E GPa	H_v (Kg/mm ²)
$\text{Sn}_{64.5}\text{Ag}_{3.5}\text{Bi}_{30}\text{In}_2$	34.5	23.13
$\text{Sn}_{64}\text{Ag}_{3.5}\text{Bi}_{30}\text{In}_2(\text{TiO}_2)_{0.5}$	29	17.82
$\text{Sn}_{63.5}\text{Ag}_{3.5}\text{Bi}_{30}\text{In}_2(\text{TiO}_2)_1$	32.83	17.62
$\text{Sn}_{63}\text{Ag}_{3.5}\text{Bi}_{30}\text{In}_2(\text{TiO}_2)_{1.5}$	28.25	17.02

The elastic constants are directly related to atomic bonding and structure. Elastic modulus and Vickers hardness values of $\text{Sn}_{87-x}\text{Sb}_{10}\text{Pb}_3(\text{TiO}_2)_x$ alloys are listed in Table 28. Elastic modulus and Vickers of $\text{Sn}_{87}\text{Sb}_{10}\text{Pb}_3$ alloy increased after adding different ratio from TiO_2 nanoparticles. Elastic modulus and Vickers hardness values of $\text{Sn}_{90-x}\text{Al}_{20}(\text{TiO}_2)_x$ ($x=0.5$ to 1.5 wt. %) alloys are listed in Table 29. Elastic modulus of $\text{Sn}_{80}\text{Al}_{20}$ alloy increased after adding different ratio from TiO_2 nanoparticles. Also, little variation occurred in Vickers hardness at 10-gram force and indentation time 5 sec of $\text{Sn}_{80}\text{Al}_{20}$ alloy after adding TiO_2 nanoparticles.

Table 28: Elastic modulus and Vickers hardness of $\text{Sn}_{64.5-x}\text{Ag}_{3.5}\text{Bi}_{30}\text{In}_2(\text{TiO}_2)_x$ alloys [30].

Alloys	E GPa	H_v (Kg/mm ²)
$\text{Sn}_{87}\text{Sb}_{10}\text{Pb}_3$	33.02	28.52
$\text{Sn}_{86.5}\text{Sb}_{10}\text{Pb}_3(\text{TiO}_2)_{0.5}$	38.3	31.68
$\text{Sn}_{86}\text{Sb}_{10}\text{Pb}_3(\text{TiO}_2)_1$	39.1	36.53
$\text{Sn}_{85.5}\text{Sb}_{10}\text{Pb}_3(\text{TiO}_2)_{1.5}$	47.2	38.83

Table 29: Elastic modulus and Vickers hardness of $\text{Sn}_{80-x}\text{Al}_{20}(\text{TiO}_2)_x$ alloys [30].

Alloys	E GPa	H_v (Kg/mm ²)
$\text{Sn}_{80}\text{Al}_{20}$	31.85	34.63
$\text{Sn}_{79.5}\text{Al}_{20}(\text{TiO}_2)_{0.5}$	37.6	35.77
$\text{Sn}_{79}\text{Al}_{20}(\text{TiO}_2)_1$	38.9	37.88
$\text{Sn}_{78.5}\text{Al}_{20}(\text{TiO}_2)_{1.5}$	40.8	

Corrosion parameters

The corrosion potential (E_{corr}), corrosion current (I_{corr}) and corrosion rate ($\text{Corr}_{\text{Rate}}$) of $\text{Sn}_{82-x}\text{Bi}_{15}\text{Zn}_3\text{Ti}_2\text{O}_x$ ($x=0.3$ to 1.2 wt. %) alloys are presented in Table 30. Corrosion rate and corrosion current of $\text{Sn}_{82}\text{Bi}_{15}\text{Zn}_3$ alloy decreased after adding (Ti_2O). The corrosion potential, corrosion current and corrosion rate of $\text{Sn}_{60}\text{Bi}_{30-x}\text{Sb}_6\text{Zn}_4\text{Cu}_{0.7}(\text{Ti}_2\text{O})_x$ ($x=0.3$ to 1.2 wt.%) alloys are listed in Table 31. Corrosion rate and corrosion current of $\text{Sn}_{60}\text{Bi}_{30}\text{Sb}_6\text{Zn}_4\text{Cu}_{0.7}$ alloy varied after adding different ratio from (Ti_2O). $\text{Sn}_{60}\text{Bi}_{28.4}\text{Sb}_6\text{Zn}_4\text{Cu}_{0.7}(\text{Ti}_2\text{O})_{0.9}$ alloy has better corrosion resistance.

Table 30: Corrosion parameters of $\text{Sn}_{82-x}\text{Bi}_{15}\text{Zn}_3\text{Ti}_2\text{O}_x$ alloys [24].

Alloys	E_{corr} mV	I_{corr} uA	$\text{Corr}_{\text{Rate}}$ mpy
$\text{Sn}_{82}\text{Bi}_{15}\text{Zn}_3$	-862	841	348.3
$\text{Sn}_{81.7}\text{Bi}_{15}\text{Zn}_3(\text{Ti}_2\text{O})$	-554	515	235.4
$\text{Sn}_{81.4}\text{Bi}_{15}\text{Zn}_3(\text{Ti}_2\text{O})_{0.6}$	-970	249	113.8
$\text{Sn}_{81.1}\text{Bi}_{15}\text{Zn}_3(\text{Ti}_2\text{O})_{0.9}$	-919	336	153.5
$\text{Sn}_{80.8}\text{Bi}_{15}\text{Zn}_3(\text{Ti}_2\text{O})_{1.2}$	-563	352	164.67

Table 31: Corrosion parameters of $\text{Sn}_{60}\text{Bi}_{30-x}\text{Sb}_6\text{Zn}_4\text{Cu}_{0.7}(\text{Ti}_2\text{O})_x$ alloys [25].

Alloys	E_{corr} mV	I_{corr} uA	$\text{Corr}_{\text{Rate}}$ mpy
$\text{Sn}_{60}\text{Bi}_{30}\text{Sb}_6\text{Zn}_4$	-913	719	328.5
$\text{Sn}_{60}\text{Bi}_{29}\text{Sb}_6\text{Zn}_4\text{Cu}_{0.7}(\text{Ti}_2\text{O})_{0.3}$	-771	190	186.83
$\text{Sn}_{60}\text{Bi}_{28.7}\text{Sb}_6\text{Zn}_4\text{Cu}_{0.7}(\text{Ti}_2\text{O})_{0.6}$	-770	283	229.3
$\text{Sn}_{60}\text{Bi}_{28.4}\text{Sb}_6\text{Zn}_4\text{Cu}_{0.7}(\text{Ti}_2\text{O})_{0.9}$	-746	186	176.77
$\text{Sn}_{60}\text{Bi}_{28.1}\text{Sb}_6\text{Zn}_4\text{Cu}_{0.7}(\text{Ti}_2\text{O})_{1.2}$	-809	604	276

The corrosion current, corrosion potential and corrosion rate of $\text{Sn}_{76}\text{Al}_{10}\text{Bi}_{10-x}\text{Cu}_2\text{Zn}_2(\text{TiO}_2)_x$ ($x=0.5$ to 1.5 wt.%) alloys in 0.25M HCl are presented in Table 32. Corrosion rate and corrosion current of $\text{Sn}_{76}\text{Al}_{10}\text{Bi}_{10}\text{Cu}_2\text{Zn}_2$ alloy decreased after adding 0.5 and 1.5wt. % titanium oxide nanoparticles but increased after adding 1wt. %.

Table 32: Corrosion parameters of $\text{Sn}_{76}\text{Al}_{10}\text{Bi}_{10}\text{Cu}_2\text{Zn}_2(\text{TiO}_2)_x$ alloys [26].

Alloys	E_{corr} mV	I_{corr} uA	Corr _{Rate} mpy
$\text{Sn}_{76}\text{Al}_{10}\text{Bi}_{10}\text{Cu}_2\text{Zn}_2$	-943	3.69	3.861e3
$\text{Sn}_{76}\text{Al}_{10}\text{Bi}_{9.5}\text{Cu}_2\text{Zn}_2(\text{TiO}_2)_{0.5}$	-873.0	3.27	3.424e3
$\text{Sn}_{76}\text{Al}_{10}\text{Bi}_9\text{Cu}_2\text{Zn}_2(\text{TiO}_2)_1$	-704.0	9.05	9.475e3
$\text{Sn}_{76}\text{Al}_{10}\text{Bi}_{8.5}\text{Cu}_2\text{Zn}_2(\text{TiO}_2)_{1.5}$	-875.0	2.92	3.085e3

Table 33 presents the corrosion potential, corrosion current, and corrosion rate of $\text{Sn}_{61}\text{Bi}_{25}\text{Sb}_5\text{Zn}_4\text{Al}_{3-x}\text{Ag}_2(\text{TiO}_2)_x$ ($x=0.3$ to 1.2 wt.%) alloys. Corrosion rate of $\text{Sn}_{61}\text{Bi}_{25}\text{Sb}_5\text{Zn}_4\text{Al}_3\text{Ag}_2$ alloy varied decreased up to 0.9wt. % titanium dioxide nanoparticle and then increased with increasing the ratio of titanium dioxide nanoparticle. That is because adding titanium dioxide nanoparticle caused heterogeneous microstructure with affected on microsegregation and reactivity of atoms with HCl solution. The $\text{Sn}_{61}\text{Bi}_{25}\text{Sb}_5\text{Zn}_4\text{Al}_{1.5}\text{Ag}_2(\text{TiO}_2)_{1.5}$ alloy has high corrosion resistance.

Table 33: Corrosion parameters of $\text{Sn}_{61}\text{Bi}_{25}\text{Sb}_5\text{Zn}_4\text{Al}_{3-x}\text{Ag}_2(\text{TiO}_2)_x$ alloys [27].

Alloys	E_{corr} mV	uA	Corr _{Rate} mpy
$\text{Sn}_{61}\text{Bi}_{25}\text{Sb}_5\text{Zn}_4\text{Al}_3\text{Ag}_2$	-857.0	1.56	1.73e3
$\text{Sn}_{61}\text{Bi}_{25}\text{Sb}_5\text{Zn}_4\text{Al}_{2.7}\text{Ag}_2(\text{TiO}_2)_{0.3}$	-776.0	3.79	3.97e3
$\text{Sn}_{61}\text{Bi}_{25}\text{Sb}_5\text{Zn}_4\text{Al}_{2.4}\text{Ag}_2(\text{TiO}_2)_{0.6}$	-825.0	8.19	8.58e3
$\text{Sn}_{61}\text{Bi}_{25}\text{Sb}_5\text{Zn}_4\text{Al}_{2.1}\text{Ag}_2(\text{TiO}_2)_{0.9}$	-539.0	152	159.1
$\text{Bi}_{25}\text{Sn}_{61}\text{Sb}_5\text{Zn}_4\text{Al}_{1.8}\text{Ag}_2(\text{TiO}_2)_{1.2}$	-797.0	3.6	3.77e3
$\text{Bi}_{25}\text{Sn}_{61}\text{Sb}_5\text{Zn}_4\text{Al}_{1.5}\text{Ag}_2(\text{TiO}_2)_{1.5}$	-587	63.4	66.35

Conclusion

Adding titanium oxide which has low density, high refractive index with higher melting temperature to tin or bismuth-based alloys improved their properties due changed its matrix structure for make it used in different industrial applications.

References

1. El-Bediwi AB, Samir R, Kamal M (2018) Electrochemical corrosion behavior, microstructure and soldering properties of tin based alloys. *Material Science Research India* 15(1): 12-22.
2. El-Bediwi AB, Khalaf MD, Omar Kh M, Meaz TM (2017) Effect of modification structure on some properties and corrosion behavior of Bi-Sn-Pb-Cd alloys for shielding blocks. *IJSRET* 3(6): 820- 826.
3. El-Bediwi AB, Bader S, Khalifa F (2016) Microstructure, electrochemical corrosion behavior and soldering properties of hexa and hepta bismuth-tin based alloy. *Global Journal of Physics* 4(3): 480- 495.
4. El-Bediwi AB, El-Shishtawi NA, Abdullah MM (2016) Study microstructure, hardness, internal friction, electrochemical corrosion and thermal behavior of tin-aluminum-antimony or tin-aluminum-bismuth based alloys. *Global Journal of Physics* 4(3): 445- 460.
5. El-Bediwi AB, Bader S, Khalifa F (2016) Effect of alloying elements on electrochemical corrosion behavior, microstructure, wettability and thermal performance of bismuth-tin based alloys. *IJSRSET* 2(2): 1267-1277.
6. El-Bediwi AB, El-Shishtawi NA, Abdullah MM (2016) Electrochemical corrosion behavior, microstructure, mechanical and thermal

performance of tin-aluminum based bearing alloys. *IJSRET* 2(2): 838-842.

7. El-Bediwi AB, Jubair MM, Shalaby RM, Kamal M (2015) Effect of adding indium on wetting behavior, microstructure and physical properties of tin- zinc eutectic alloy. *International Journal of Science and Engineering Applications* 4(4): 186-190.
8. El-Bediwi AB, El-Shafei A, Kamal M (2015) Study the effect of adding bismuth or bismuth-indium on structure and physical properties of eutectic tin-copper alloy. *Global Journal of Physics* 2(1): 67-78.
9. El-Bediwi AB, Dawood F, Kamal M (2015) New hexa bismuth- tin based alloys for electrical fuse and nuclear applications. *International Journal of Current Research* 7(5): 16433-16439.
10. El-Bediwi AB, Al-Bawee A, Kamal M (2015) Corrosion behavior and physical properties of modified tin-antimony bearing alloy. *MSAIJ* 13(4): 136-144.
11. El-Bediwi AB, Dawood F, Kamal M (2015) Effect of quaternary addition on structure, electrical, mechanical and thermal properties of bismuth-tin-zinc rapidly solidified fusible alloy. *Journal of Advances in Physics* 7(3): 1952-1958.
12. El-Bediwi AB, El-Shafei A, Kamal M (2014) Influence of adding bi\or bi-in on structure and required properties of tin-copper lead free solder alloy. *International Journal of Engineering & Technology* 14(6): 61-68.
13. El-Bediwi AB, Kashita E (2013) Effects of alloying elements on physical properties of tin-antimony based lead free solder alloys. *MSAIJ* 9(5): 163-167.
14. El-Bediwi AB (2005) Correlation of structure and properties of melt spun $\text{PbSn}_{30}\text{Sb}_7\text{Cu}$ quaternary alloys. *Cryst Res Technol* 40(7): 688-691.
15. El-Bediwi AB, El-Bahay MM (2004) Influence of sliver on structural, electrical, mechanical and soldering properties of tin-indium based alloys. *Radiation Effect & Defects in Solids* 159(2): 133-140.
16. El-Bediwi AB (2003) Effects of micro -addition on structures and properties of rapidly solidified Sn-10%Sb alloy. *Radiation Effect & Defects in Solids* 158(7): 475-479.
17. El-Bediwi AB (2002) Effect of ternary addition and cooling rate on the structure and properties of Lead-Tin based alloy. *AMSE* 75(3-4).
18. Glazer J (1994) Microstructure and mechanical properties of Pb-free solder alloys for low-cost electronic assembly: A review. *Journal of Electronic Materials* 23(8): 693-700.
19. Shiue RK, Tsay LW, Lin CL, Ou JL (2003) A study of Sn-Bi-Ag-(In) lead-free solders. *J Mater Sci* 38(6): 1269-1279.
20. Osório WR, Peixoto LC, Garcia LR, Noël NM, Garcia A (2013) Microstructure and mechanical properties of Sn-Bi, Sn-Ag and Sn-Zn lead-free solder alloys. *J Alloy Compd* 572: 97-106.
21. Shepelevich VG, Gusakova OV, Shcherbachenko LP (2013) Structure and properties of rapidly solidified Sn-58 wt % Bi foils. *Inorganic Mater* 49(7): 663-667.
22. Esfandyarpour MJ, Mahmudi R (2011) Microstructure and tensile behavior of Sn-5Sb lead-free solder alloy containing Bi and Cu. *Mate Sci Eng: A* 530: 402-410.
23. Mc Cormack M, Chen HS, Kammalott GW, Jin S (1997) Significantly improved mechanical properties of bi-sn solder alloys by ag- doping. *J Electron Mater* 26(8):954-958.
24. El-Bediwi AB, Samir R (2018) Influence of titanium oxide on structure, corrosion and soldering properties of $\text{sn}_{82}\text{bi}_{15}\text{zn}_3$ alloy. *Res Dev Material Sci* 6(1): 1-8.
25. El-Bediwi AB, Samir R. Effect of titanium oxide nanopartiles on corrosion behavior and solder properties of penta tin- bismuth based alloy.

26. El-Bediwi AB, El-Shishtawi NA, Abdullah MM (2016) Influence of titanium dioxide nanoparticles on microstructure, electrochemical corrosion behavior, mechanical and thermal properties of Sn-Al-Bi based alloy. *International Journal of Applied Science and Biotechnology* 4(3): 417-424.
27. El-Bediwi AB, Bader S, Khalifa F (2016) Study the effect of titanium dioxide on microstructure, electrochemical corrosion parameters, thermal behavior and internal friction of hexa tin-bismuth based alloy. *Mat Sci Ind J* 14(13): 1-19.
28. El-Bediwi AB, Grayb M, Kamal M (2015) Influence of titanium oxide on creep behavior, microstructure and physical properties of tin-antimony and tin-aluminum-antimony based bearing alloys. *International Journal of Science and Engineering Applications* 4(2): 64-70.
29. El-Bediwi AB, El-Shafei A, Kamal M (2015) New tin-bismuth based lead free solder alloys with superior properties for industrial applications. *International Journal of Current Research* 7(6): 17305-17311.
30. El-Bediwi AB, Abbas Al-Bawee, Kamal M (2015) Effect of titanium oxide on structure, bearing properties of tin-antimony-lead and tin-aluminum alloys. *International Journal of Science and Engineering Applications* 4(2): 46-53.
31. Geranmayeh AR, Mahmudi R (2005) Power law indentation creep of Sn-5% Sb solder alloy. *J Matter Sci* 40(13): 3361-3366.
32. Kangooie M, Mahmudi R, Geranmayeh AR (2010) Impression creep of a lead-free Sn-1.7Sb-1.5Ag solder reinforced by submicron-size Al_2O_3 particles. *J Electr Matter* 39(2): 215-222.
33. Rani SD, Murthy GS (2004) Impression creep behaviour of tin based lead free solders. *Mate Sci Techn* 20(3): 403-408.

For possible submissions Click below:

[Submit Article](#)